J Mater Sci (2017) 52:11554–11568

Electronic materials

Enhancement of the acetone sensing capabilities to *ppb* detection level by Fe-doped three-dimensional SnO_2 hierarchical microstructures fabricated via a hydrothermal method

Jie Hu[1,*], Ying Wang[1], Wenda Wang[1], Yan Xue[1], Pengwei Li[1], Kun Lian[1], Lin Chen[2,*], Wendong Zhang[1], and Serge Zhuiykov[3]

[1] *Micro and Nano System Research Center, Key Lab of Advanced Transducers and Intelligent Control System (Ministry of Education) and College of Information Engineering, Taiyuan University of Technology, Taiyuan 030024, Shanxi, China*

[2] *Research Center on Advanced Materials Science and Technology, Taiyuan University of Technology, Taiyuan 030024, China*

[3] *Department of Applied Analytical and Physical Chemistry, Faculty of Bioscience Engineering, Ghent University Global Campus, 119 Songdomunhwa-ro, Yeonsu-gu, Incheon 21985, South Korea*

Received: 1 April 2017
Accepted: 23 June 2017
Published online: 28 June 2017

ABSTRACT

Acetone detection at the parts-per-billion (ppb) level is achieved in this work using selective and optimized Fe doping of the three-dimensional (3D) flower-like SnO_2 hierarchical microstructures. These structures were successfully synthesized via a one-step hydrothermal route. Detailed information about the crystal structure, surface morphology and composition of the Fe-doped SnO_2 microstructures was investigated using X-ray diffraction (XRD), energy-dispersive spectroscopy (EDS), scanning electron microscopy (SEM), transmission electron microscopy (TEM) and X-ray photoelectron spectroscopy (XPS) techniques. Gas sensing experiments were conducted on the as-prepared Fe-doped SnO_2 sensors. The measured results show that the incorporation of Fe into the SnO_2 structure can greatly enhance the gas sensing properties of SnO_2 sensors under the optimum working temperature (200 °C). Specifically, the 1.0 mol% Fe-doped SnO_2 microstructures exhibit the highest response, fast response/recovery time, lowest detection limit and good selectivity and long-term stability. The results demonstrate that the developed Fe-doped SnO_2 gas sensor has great potential for *ppb*-level acetone detection in many practical applications.

Address correspondence to E-mail: hujie@tyut.edu.cn; chenlin01@tyut.edu.cn

DOI 10.1007/s10853-017-1319-8

Introduction

Acetone is a highly flammable gas which has been widely used in industries and scientific laboratories. Research indicates that people exposure to the high acetone concentration (more than 173 ppm) may cause low blood pressure, bronchial irritation, difficulty breathing and abdominal pain [1, 2]. Therefore, it is very important to detect the concentration of acetone at the workplace to ensure safety and health. Apart from that, being an important breath biomarker, the exhaled acetone level has been recognized to possess tight and quantitative connection with the human diabetes. Generally, gaseous acetone concentration in breath varies between 300 and 900 ppb in healthy people, while the concentration in diabetes patients is reported to exceed 1.8 ppm [3]. Thus, in order to achieve accurate disease diagnosis using exhaled breath sensors, the detection limit should be at ppb level, especially in highly humid atmospheres. Up to now, although considerable efforts have been devoted to acetone detection using analysis equipment such as gas chromatography/mass spectrometry (GC/MS) [4] and optical spectroscopy [5], these techniques still suffer from disadvantages such as bulky size, high cost and time-consuming measurement. These drawbacks limit wider applications of the existing acetone detection techniques [6]. Therefore, it is highly desirable to develop high-performance miniature sensors for the rapid and selective detection of acetone in practical applications.

Recently, considerable efforts have been made to develop gas sensors using various oxide semiconductors including SnO_2 [7, 8], WO_3 [9, 10], In_2O_3 [11], ZnO [12], NiO [13], MnO_2 [14], V_2O_5 [15]. In particular, SnO_2 (an n-type semiconductor with a wide band gap (3.6 eV)) is one of the most studied due to its better performance and high chemical stability [16]. However, most sensors based on bulky SnO_2 still suffer from numerous problems associated with relatively poor sensitivity, long response/recovery time and low reliability [17, 18]. They still can't meet these growing demands for fast-responding, accurate and reliable sensors with ppb-level detection. Therefore, great efforts have been dedicated to further improve the acetone sensing capabilities, such as improvement of the specific surface area, formation the heterojunction structure and doping with extrinsic dopants [19–21]. Noteworthy, doping with extrinsic dopants has been demonstrated as a facile and effective way to improve the sensitivity of SnO_2-based sensors. It was recently reported that Zn-doped SnO_2 nanostructures exhibited tremendous sensing performance toward glycol where the sensor's response to 100 ppm glycol was about two times higher than that of undoped SnO_2 sensor [22]. It was also demonstrated that NiO-doped SnO_2 polyhedra has a significantly enhanced response of 6.7–30 ppm ethanol at 280 °C with the response and recovery times were shorter than 0.6 and 10 s, which are much better than that of pure SnO_2 [23]. In addition, there are many other reports about doping nanostructured SnO_2 resulted in the significant improvement of the sensor's characteristics [24, 25]. All of those reports confirm the feasibility of successful doping of SnO_2 by nanostructured dopants to achieve the desired improvements. Despite the tremendous research on the influence of doping on sensing performances, only few of the recent reports touched on the optimization of Fe content which might be critical for SnO_2 gas sensing performance.

Herein, both pure SnO_2 and different contents of Fe-doped 3D flower-like hierarchical SnO_2 microstructures were successfully synthesized by the hydrothermal process. Their crystal structure, surface morphology and composition were subsequently characterized. Meanwhile, the acetone sensing experiments were conducted on the pure and Fe-doped SnO_2 sensing materials. The measured results clearly show that the incorporation of Fe into the structure of SnO_2 can greatly improve the gas sensing performances of SnO_2-based acetone sensors. In particular, the 1.0 mol% Fe-doped SnO_2 microstructures exhibited the highest response, best selectivity and excellent long-term stability, which indicate that the Fe-doped 3D SnO_2 microstructures can be utilized as a promising sensing material for detection of *ppb*-level acetone gas.

Experimental

Materials and reagents

Tin chloride dihydrate ($SnCl_2{\cdot}2H_2O \geq 99.9\%$) and ferric chloride hexahydrate ($FeCl_3{\cdot}6H_2O \geq 99.0\%$) were purchased from Sigma–Aldrich (Shanghai,

China). Sodium citrate dihydrate ($C_6H_5Na_3O_7{\cdot}2H_2O \geq 99.0\%$) was obtained from Aladdin Chemistry Co., Ltd. (Shanghai, China). All chemical reagents in this experiment were of analytical grade and used without further purification.

Synthesis of flower-like hierarchical SnO_2 microstructures

Pure and Fe-doped SnO_2 microstructures were synthesized by hydrothermal method. Typically, 4 mmol $SnCl_2$ $2H_2O$, 10 mmol $C_6H_5Na_3O_7$ $2H_2O$ and a definite amount of $FeCl_3$ $6H_2O$ (Fe/Sn = 0.5 mol%, 1.0 mol%, 3.0 mol%) were dissolved into 40 mL of an ethanol–water (2:3, v/v) solution magnetic string for 10 min to form a homogeneous solution. Subsequently, the resultant mixture solution was transferred into a 100-mL Teflon-lined stainless steel autoclave and heated at 210 °C for 12 h. After it was cooled down to room temperature, the obtained precipitates were washed thoroughly by adding deionized water and ethanol, followed by centrifugation at 6000 rpm for 5 min. Finally, the products were annealed at 600 °C for 2 h with a ramping rate of 3 °C min^{-1}. Furthermore, the pure SnO_2 microstructures were also synthesized using the same method without addition of $FeCl_3$ $6H_2O$ in the solution.

Characterization

The obtained SnO_2 microstructures were examined in terms of their morphological, crystalline structural, compositional properties. The crystal structure and the phase of the as-synthesized products were measured by X-ray diffractometer (XRD, DRIGC-Y 2000A) with Cu-Kα_1 radiation ($\lambda = 1.5406$ Å) in the range of 20°–80°. The surface morphologies and microstructures of the obtained samples were investigated by field-emission scanning electron microscopy (FESEM, JEM-7100F, operated at 20 kV) and a high-resolution transmission electron microscope (HRTEM, JEM-2010, 200 kV with electron diffraction). The chemical composition elements of the product were analyzed by the energy-dispersive spectroscopy (EDS, QUANTAX200). The surface composition and the chemical state of samples were studied by X-ray photoelectron spectroscope (XPS, ESCALAB 250Xi) with Al Ka X-ray radiation at 15 kV. All XPS spectra were accurately calibrated using the C 1 s peak of graphitic carbon at 284.6 eV as a reference. The current–voltage (I-V) characteristics of prepared sensors were tested using the semiconductor device analyzer (Agilent Technologies B1500A).

Fabrication and measurement of gas sensors

The structure of the gas sensor belongs to the side-heated type. The fabrication process of acetone sensor is as follows: The calcined product was firstly mixed with suitable amount of ethyl cellulose and terpineol (weight ratio 2:1:8) and hand-ground in an agate mortar to form a small amount of slurry. Secondly, the paste was coated on the surface of cylindrical Al_2O_3 ceramic tube installed with a pair of Au electrodes and Pt wires. After that, the sensing elements were dried at the room temperature and annealed at 600 °C for 2 h. Then, a Ni–Cr heating wire was inserted into the tube to control the operating temperature. Finally, the sensing element was welded onto the pedestal formation the gas sensor. The gas sensing properties of the as-prepared pure and Fe-doped SnO_2 sensors were tested using CGS-1TS intelligent analysis system (Elite, Beijing, China). The relative humidity in the measurement atmosphere was maintained at about 35 ± 2%. The sensor response (S) is defined as the ratio (Ra/Rg) of the sensor resistance in air (Ra) to that in target gases (Rg). The time taken for the sensor to achieve 90% of the total resistance change was defined as the response time in the case of adsorption or the recovery time in the case of desorption [26].

Results and discussion

Structural and morphological characteristics

Figure 1a shows the XRD patterns of all samples after annealing at 600 °C. The measured results exhibit that all of the detected diffraction peaks are well matched with the tetragonal SnO_2 structure (JCPDS card no. 41-1445). In addition, no obvious XRD peaks of Fe element are observed in the Fe-doped SnO_2 microstructures, which may be due to the low concentration of Fe in the samples. Figure 1b shows the magnified region of the (110) peaks for the Fe-doped SnO_2 microstructures. All the measured diffraction angles shift to larger value with the increasing Fe

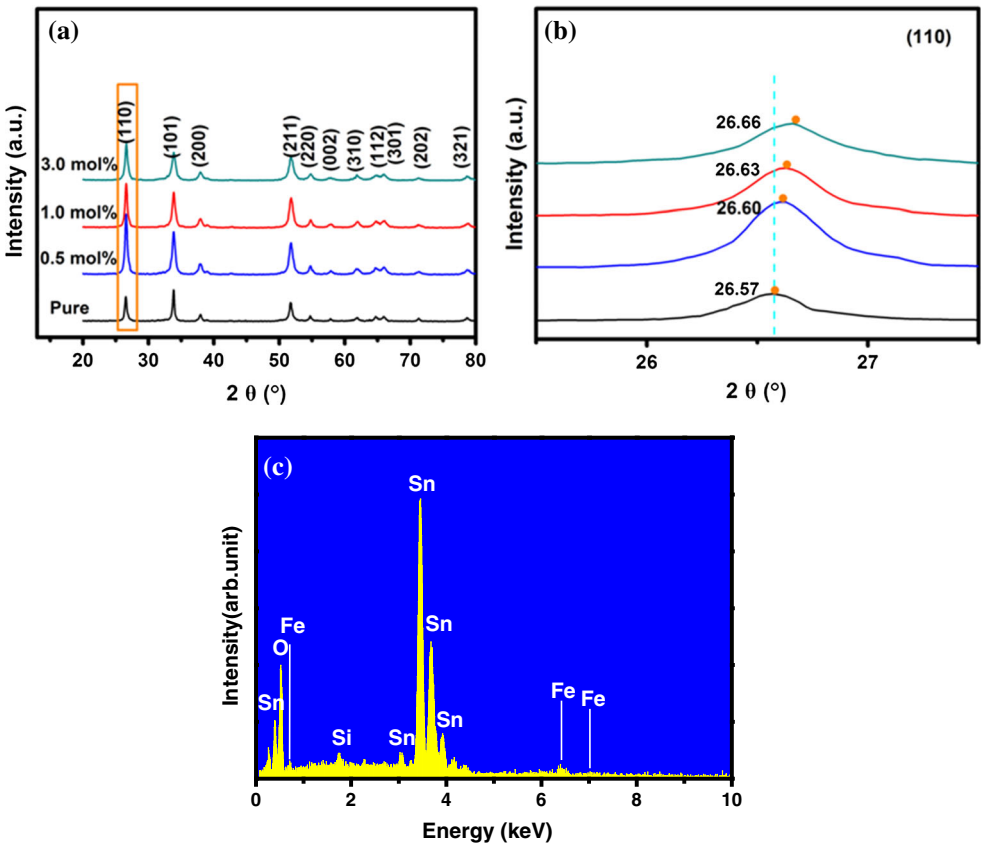

Figure 1 XRD patterns of as-synthesized samples for **a** pure and Fe-doped SnO_2 microstructures, **b** high magnification of the (110) peak, **c** EDS spectrum of 3.0 mol% Fe-doped SnO_2 sample.

concentration. Table S1 (Supporting information) illustrates the details of the peak position, which indicates that the Sn ions were partially substituted by Fe ions in the samples. Similar results have been previously demonstrated [21, 27, 28]. In the air, Fe_3O_4 can be converted into Fe_2O_3 via heat treatment at 450 °C or higher, which indicates that Fe^{2+} can be converted into Fe^{3+} at temperatures above 450 °C [29]. All samples prepared were subsequently calcined at 600 °C for 2 h in air prior to gas sensing tests, to ensure that the doping into SnO_2 lattice was Fe^{3+} ions. In addition, the element composition for 3.0 mol% Fe-doped SnO_2 was examined by EDS analysis (Fig. 1c). As a result, only Fe, Sn and O elements existed in the sample, which suggests a high level of purity of the sintered microstructures. Meanwhile, the chemical compositions of Fe-doped SnO_2 samples were qualitative analyzed as shown in Fig. S2 (Supporting information), and the atomic percentage of Fe element in 0.5, 1.0, 3.0 mol% Fe-doped SnO_2 samples is 0.438, 0.812 and 2.842 at.%, respectively.

The surface morphologies and microstructures of pure SnO_2 and Fe-doped SnO_2 were observed by SEM as shown in Fig. 2. The results show that the flower-like pure SnO_2 microstructures appear to be assembled together by numerous SnO_2 nanosheets with the average size of approximately 2–3 μm (Fig. 2a). After the introduction of the Fe dopant, it seems that there was no apparent influence of the dopant on both the morphology and dimensions of the developed SnO_2 microstructures, as shown in Fig. 2b–d. Furthermore, the SEM micrograph and EDS elemental mapping were performed on the 3.0 mol% Fe-doped SnO_2 sample and the results are illustrated in Fig. 2e–h. The corresponding elemental mapping images of tin, oxygen and iron reveal an identical spatial distribution, which suggests that the Fe element is immobilized at the surface of the SnO_2 microstructures.

The morphology and microstructure of the synthesized SnO_2 samples were further characterized by TEM and high-resolution TEM (HRTEM). Figure 3a depicts the representative TEM images of 3.0 mol% Fe-doped SnO_2. The HRTEM image of the Fe-doped SnO_2 microstructure is shown in Fig. 3b, which indicates that the inter-planar spacing of the lattice fringes is 0.238 and 0.264 nm, respectively,

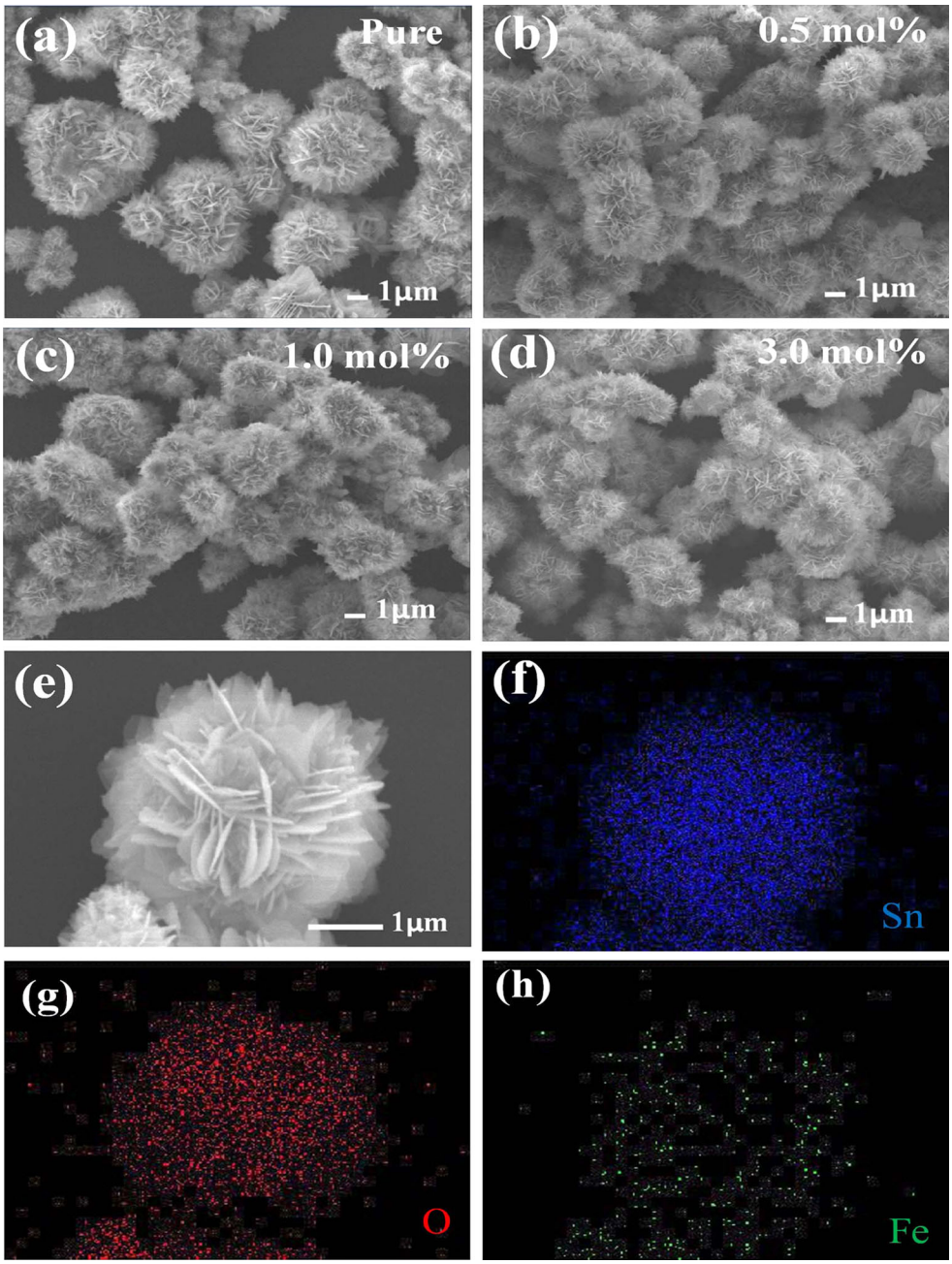

Figure 2 SEM images of as-prepared samples for **a** pure SnO_2, **b** 0.5 mol%, **c** 1.0 mol%, **d** 3.0 mol% Fe-doped SnO_2 microstructures, **e**–**h** element mapping of 3.0 mol% Fe-doped SnO_2 sample.

corresponding to the (200) and (101) crystal planes of tetragonal SnO_2 structure. As shown in Fig. 3c, the lattice fringe spacing of the small nanoparticle on the SnO_2 nanosheet was observed to be 0.208 nm corresponding to the (202) plane of α-Fe_2O_3, while the lattice fringe spacing in nanosheet was 0.335 nm corresponding to the (110) plane of SnO_2. A higher-magnification HRTEM image of the same sample (Fig. 3d) exhibits sets of lattice fringes with an interplanar distance of 0.367 nm, which is attributed to the (110) plane of α-Fe_2O_3. These results reveal that the Fe_2O_3 nanoparticles were successfully incorporated into the surface of SnO_2, which is consistent with the previous XRD and EDS analysis.

The chemical composition and chemical valence of the 3.0 mol% Fe-doped SnO_2 sample were measured by XPS as shown in Fig. 4. In the full range of the XPS spectrum (Fig. 4a), the binding energies correspond

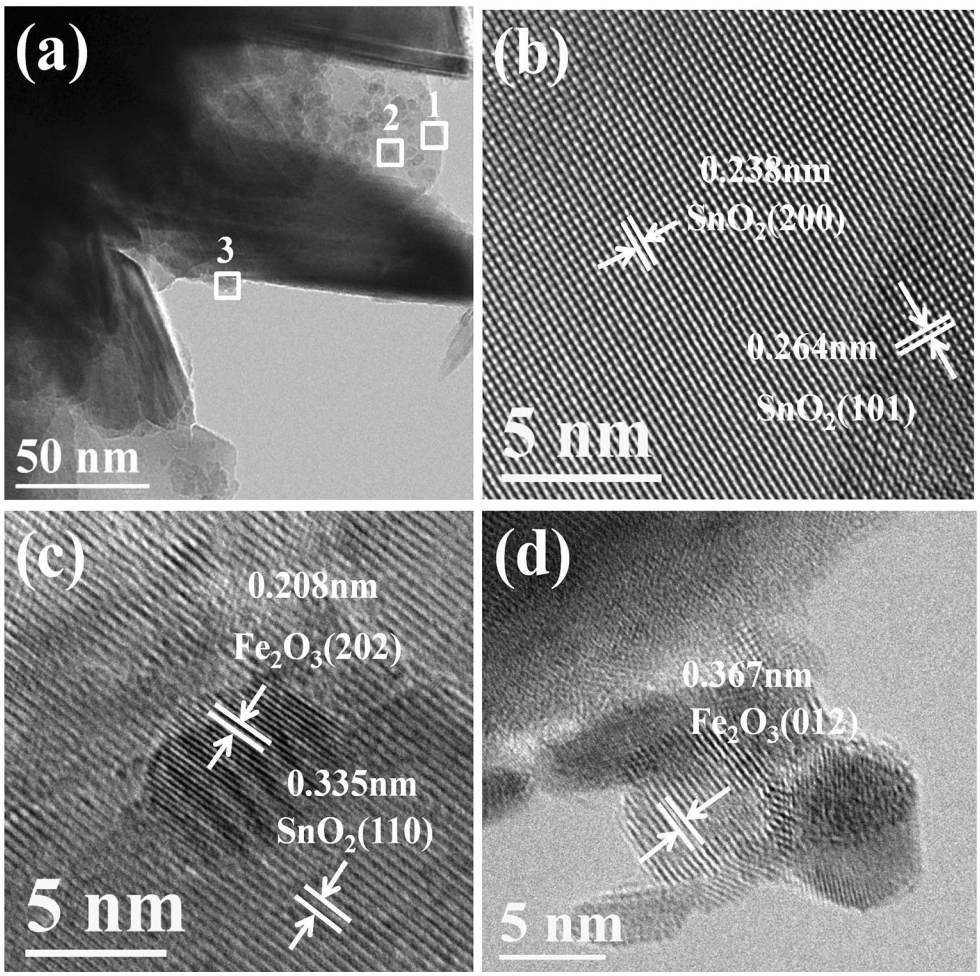

Figure 3 TEM images of **a** 3.0 mol% Fe-doped SnO_2 microstructures, **b**–**d** HRTEM image of **b** SnO_2 and Fe_2O_3 lattice fringes.

to different energy levels of O, Sn and C, which are clearly observed. However, no obvious impurities other than carbon could be found in the spectrum. From Fig. 4b, we can find that the peak positions of Sn $3p_{3/2}$ at 716.25 eV located at around 716.25 eV and 464.1 eV, respectively, which is attributed to Sn^{4+} in the SnO_2 lattice. Noteworthy, two very weak peaks at the lower binding energy of 711.3 and 724.6 eV were corresponded to the characteristic doublet of Fe $2p_{3/2}$ and Fe $2p_{1/2}$ spectrum of Fe_2O_3, implying that the oxide state of iron is trivalent [30]. Moreover, the binding energy of 56.2 eV could be ascribed to Fe 3p, as depicted in Fig. 4c. With respect to O 1 s (Fig. 4d), its core-level spectrum was resolved into three peaks at 530.3, 531 and 532 eV, respectively. The peak at the lower binding energy of 530.3 eV corresponded to the SnO_2 lattice oxygen. The medium binding energy of 531 eV is assigned to the O^{2-} ions in the oxygen deficient regions. For the high binding energy (532 eV), it could be attributed to the presence of oxygen ions chemisorbed on the SnO_2 surface. As discussed above, the XPS results further confirmed that the Fe dopants were incorporated into SnO_2 products.

Gas sensing properties

It is well known that the working temperature plays a critical role in the response of a semiconductor gas sensor [31]. That's why initially both pure SnO_2 and Fe-doped SnO_2-based sensors were investigated for the detection of 100 ppm acetone at different operating temperatures ranging from 125 to 275 °C, in order to optimize the working temperature where the highest sensing capabilities can be obtained. Figure 5 shows that the responses of all sensors increased as the temperature increased to 200 °C, and then decreased dramatically. This phenomenon can be

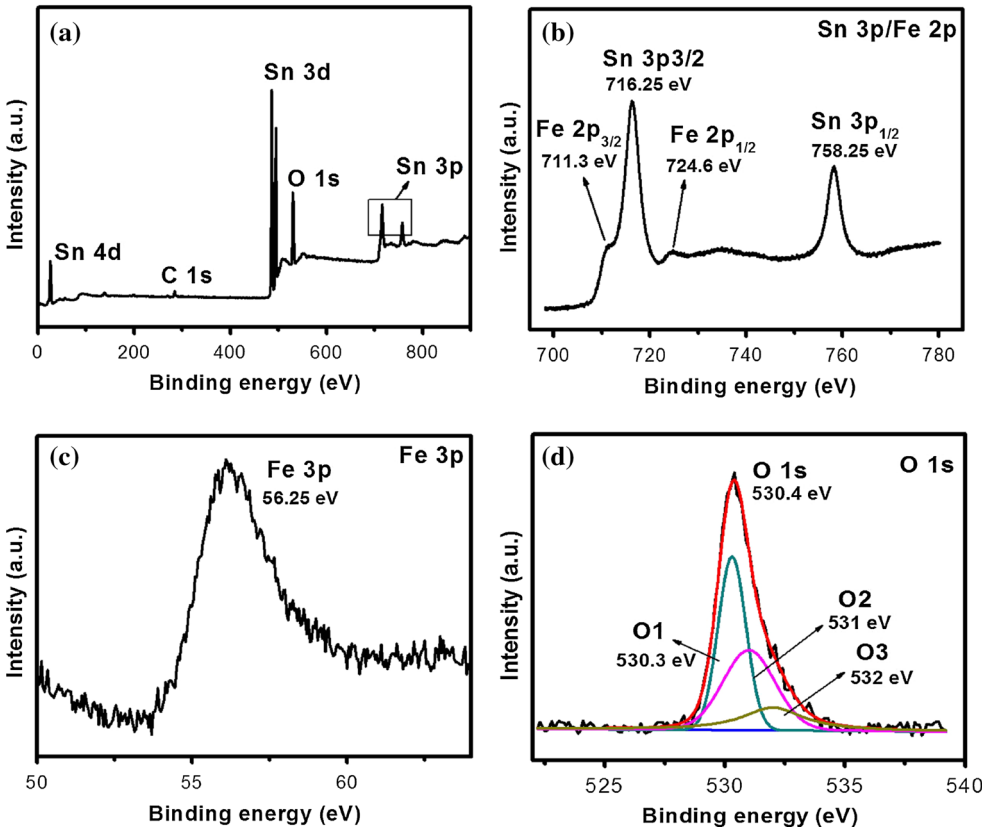

Figure 4 XPS survey spectra of **a** 3.0 mol% Fe-doped SnO_2 sample, **b** Sn 3p/Fe2p, **c** Fe 3p, **d** O 1 s.

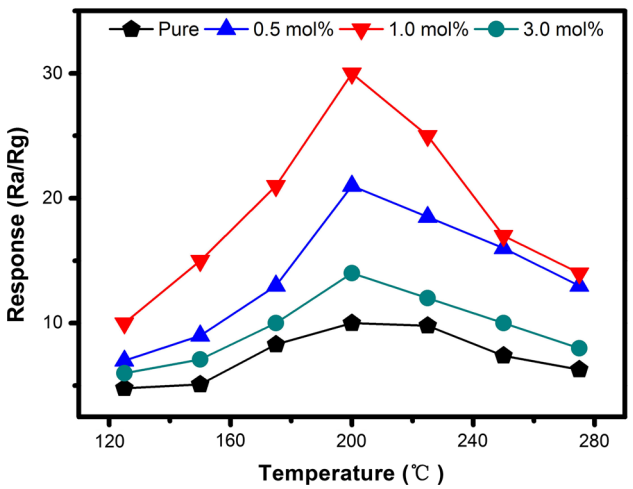

Figure 5 Temperature-dependent response curve of the as-prepared pure SnO_2 and Fe-doped SnO_2 gas sensors toward 100 ppm acetone.

ascribed to both thermodynamics and kinetics of the acetone adsorption and desorption on the surfaces of the sensors [32, 33]. When the semiconductor-based sensor works at the lower temperatures, the thermal energy of the gas molecules is too low to react with the surface-adsorbed oxygen species [34, 35]. However, as the temperature increases, the thermal energy obtained is high enough to overcome the potential barrier of the surface reaction. Moreover, the electron concentration increases due to the conversion of adsorbed oxygen species, which facilitates the chemical reaction and leads to a stronger response. On the contrary, under the higher temperatures, the adsorption ability of gas molecules decreased causing the low utilization rate, which in turn leads to the decrease in the sensor's response. Clearly, 200 °C is the optimum working temperature for the as-fabricated samples, and unless we stated otherwise, all following measurements were carried out at 200 °C. In addition, it was discovered that the 1.0 mol% Fe-doped SnO_2 sensor exhibits the highest response to 100 ppm acetone under the optimum working temperature of 200 °C, which is almost three times higher than the response of the pure SnO_2-based sensor. Meanwhile, the response of the sensor based on SnO_2 microstructures to 100 ppm ethanol was also measured under the different operating temperatures. The results have also show that the 1.0 mol% Fe-doped SnO_2 sensor has excellent sensing

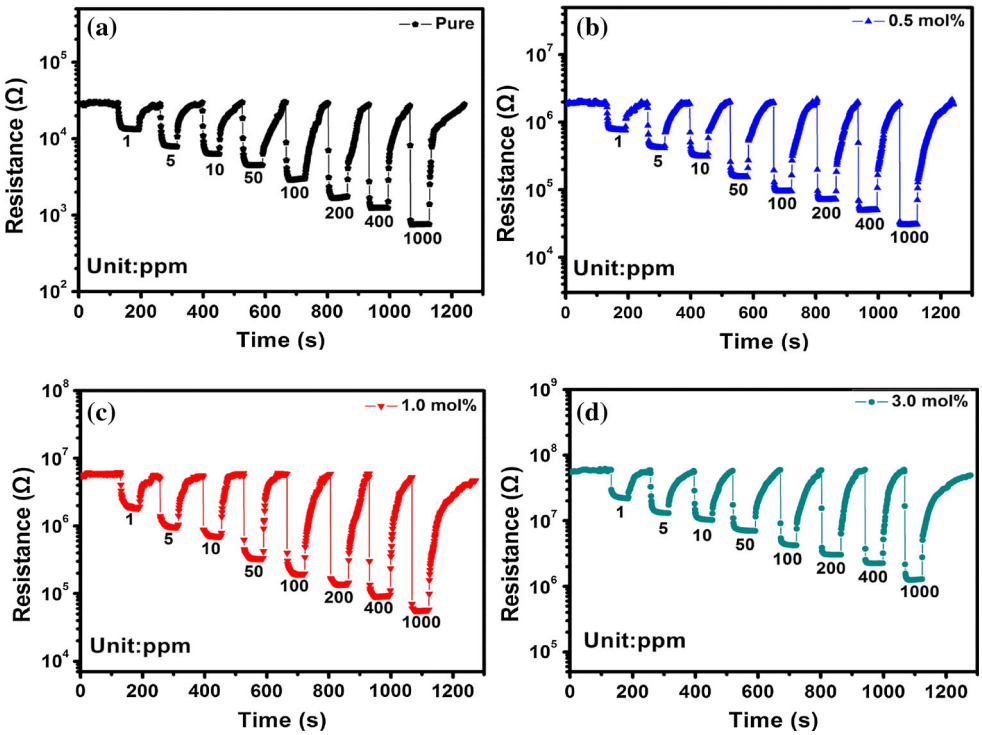

Figure 6 Dynamic response–recovery curves of the as-fabricated gas sensors to different concentrations of acetone at optimum working temperature, **a** pure SnO_2, **b** 0.5 mol%, **c** 1.0 mol%, **d** 3.0 mol% Fe-doped SnO_2 microstructures.

properties for ethanol (Fig. S3 in Supporting information).

To further investigate the sensing properties of as-prepared gas sensors, dynamic resistance transient experiments were conducted on both pure SnO_2 and Fe-doped SnO_2-based sensors at the optimum working temperature. Figure 6a–d displays the dynamic transient curves for all sensors for different acetone concentrations (1, 5, 10, 50, 100, 200, 400 and 1000 ppm) at 200 °C. It can be seen that the resistance of the gas sensors decreases sharply when the target gas (acetone) was injected into the chamber. It reverts to the initial value after exposure to fresh air. Noteworthy, the measured resistances of the sensors also decreased significantly with the increase in acetone concentration. The initial resistance of as-prepared sensors increases with the increase in Fe content in SnO_2, which indicates that the introduction of Fe element has indeed a significant influence on sensor's characteristics. Meanwhile, there was no apparent "baseline drift" observed for all sensors, which confirmed the great repeatability of their performance. In addition, all as-fabricated gas sensors were further tested investigate to the different ethanol concentrations and the results are presented in Fig. S4 (Supporting information). All of the above results have clearly demonstrated that the sensor based on Fe-doped SnO_2 3D microstructure exhibits superior sensing capabilities compared with the sensor based on pure SnO_2.

To find out the lowest acetone detection level for the Fe-doped SnO_2 3D microstructure, further tests were carried out at the optimum working temperature of 200 °C and the main results are shown in Fig. 7. It is evident that the sensors based on Fe-doped SnO_2 3D microstructures exhibit better response/recovery to *ppb* level of acetone compared with sensors based on pure SnO_2. Specifically, 1.0 mol% Fe-doped SnO_2 sensor showed superior acetone sensing performance than the others, and the measured response reached to 1.55 even at 100 ppb acetone at 200 °C. The lowest acetone detection limit (LOD) was estimated with $Ra/Rg > 1.2$ being used as the criterion for gas detection [36, 37]. When the acetone concentration is 100 ppb, the corresponding sensitivity $(Ra/Rg) = 1.55 > 1.2$. Therefore, it is appeared to indicate the detection limit of the sensor based on 1.0 mol% Fe-doped SnO_2 could be as low as 100 ppb. Consequently, this doped nanomaterial can be considered as promising candidate for sensors measuring traces of acetone in many practical applications.

Figure 8 plots linear fits for all types of sensors toward acetone with concentration range from 100 to

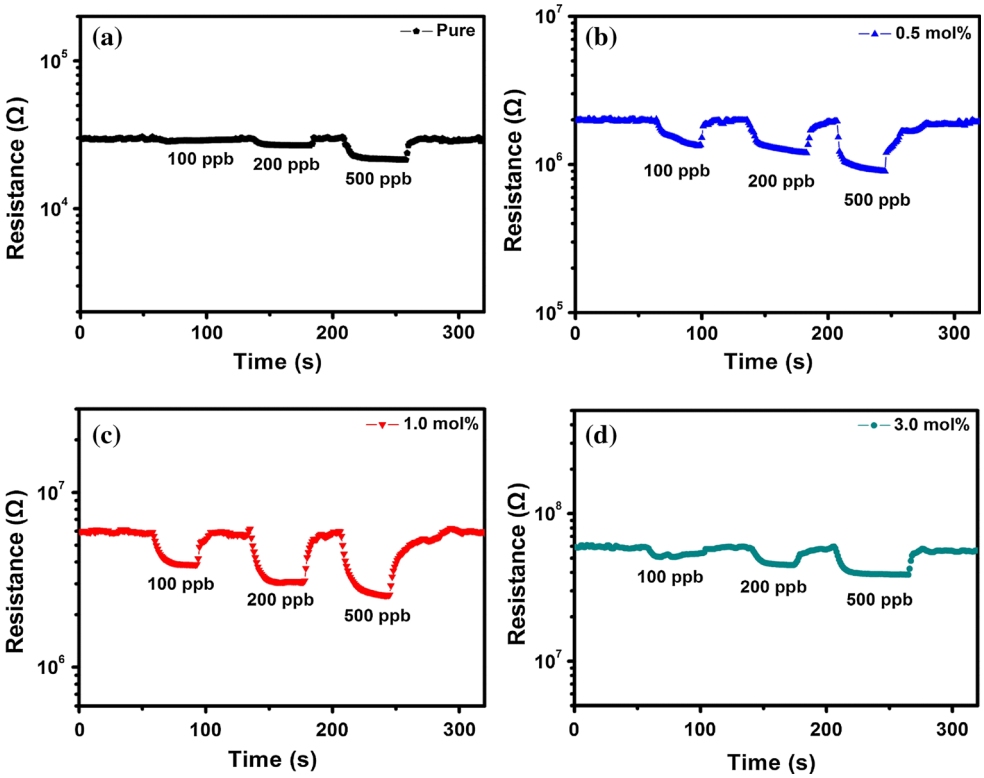

Figure 7 Dynamic resistance curves of gas sensors to low concentrations of acetone (100–500 ppb) at 200 °C, **a** pure SnO_2, **b** 0.5 mol%, **c** 1.0 mol%, **d** 3.0 mol% Fe-doped SnO_2 microstructures.

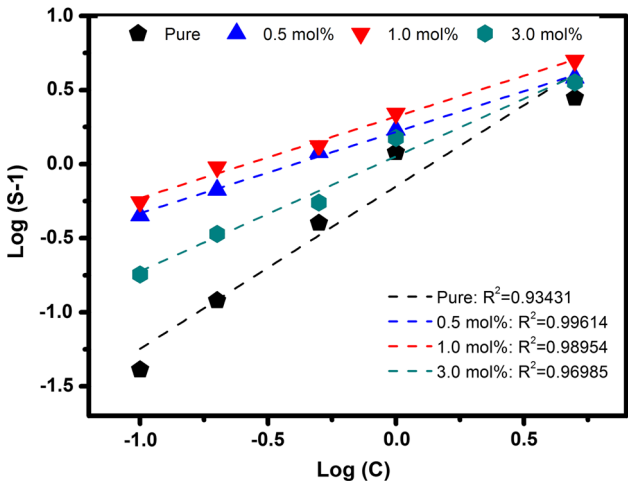

Figure 8 Linear fitting of as-prepared pure and Fe-doped SnO_2 gas sensors.

5 ppm. An empirical equation is often used to relate the response of a metal oxide semiconductor and the target gas concentration: $S = 1+a[C]^b$ [38, 39], where a and b are constants, C the target gas concentration. The equation can be rewritten in a linear form: $\log (S–1) = b\log (C) + \log (a)$. The measured results demonstrated that both pure and Fe-doped SnO_2 gas sensors show good linear relationships. In particular, the correlation coefficient (R^2) of the 1.0 mol% Fe-doped SnO_2 sensor is about 0.98954, which exhibits the best linear relationship for acetone detection.

In practical applications, it is required that acetone sensors should have quick response and recovery time. Therefore, the response/recovery characteristics of the acetone sensors based on pure and Fe-doped SnO_2 3D microstructures for 100 ppm acetone were investigated at the optimum working temperature. Figure 9a illustrates the dynamic response–recovery characteristics of 1.0 mol% Fe-doped SnO_2 sensor at 200 °C. The measured results showed that the response and recovery times for 1.0 mol% Fe-doped SnO_2 sensor were about 1 and 58 s, respectively. In addition, Fig. 9b depicts the response and recovery time to 100 ppm acetone of all acetone sensors based on Fe-doped SnO_2 with different concentration of the dopant. These measurements show that response/recovery times are similar to the most of the sensors with exception to the sensor based on

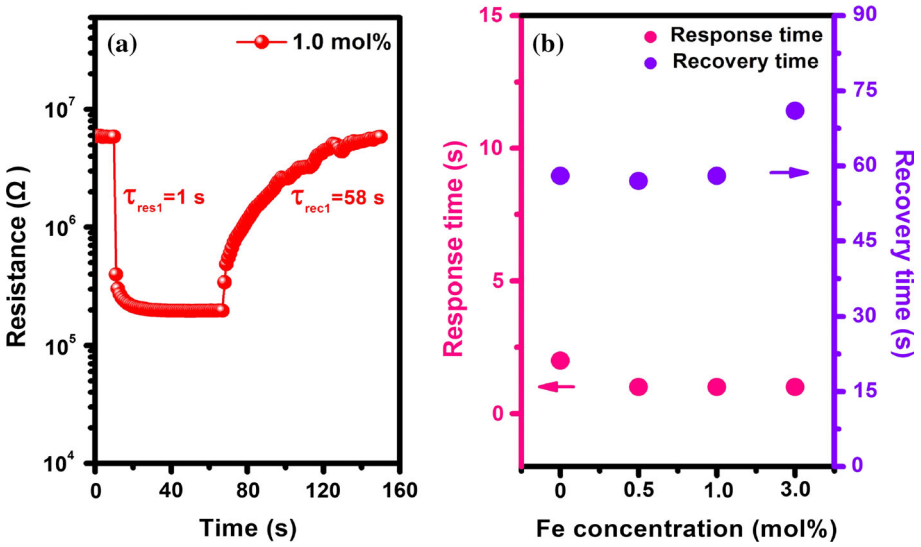

Figure 9 Transient resistance of **a** pure and 1.0 mol% Fe-doped SnO_2 microstructures to 100 ppm acetone at 200 °C, **b** response and recovery time of as-prepared gas sensors toward 100 ppm acetone at 200 °C.

3.0 mol% Fe-doped SnO_2. The longer recovery time for this sensor may be attributed to the adsorption/desorption speed of acetone molecules on the surface of sensing material [40].

Meanwhile, the current–voltage (I-V) characteristics were conducted on the 1.0 mol% Fe-SnO_2 sensor using semiconductor device analyzer, as shown in Fig. 10. When the as-fabricated gas sensor was exposed into air (without acetone gas), the measured current is about 0.16 μA under the applied voltage of 4 V. However, after injection into 100 ppm acetone gas, the measured current can reach to 21.5 μA for 1.0 mol% Fe-doped SnO_2 sensor. The enhancement of conductance for the sensor can be attributed to the increases in the charge carriers after exposure into acetone gas. The similar results have been reported in previous work [41].

As the selectivity is also one of the main characteristics of gas sensors, it was also tested. All sensors were exposed to 100 ppm of various gases at 200 °C, such as acetone (CH_3COCH_3), ethanol (C_2H_5OH), ammonia (NH_3), hydrogen (H_2), carbon monoxide (CO), methanol (CH_3OH) and methane (CH_4). Figure 11 shows the selectivity of the pure and Fe-doped SnO_2 microstructures sensors to different gases. It can be clearly observed that all sensors showed very low responses upon exposure to gases CH_4, CO, H_2, NH_3, while the major response was detected for the measuring acetone. It is also clear that the 1.0 mol% Fe-doped SnO_2

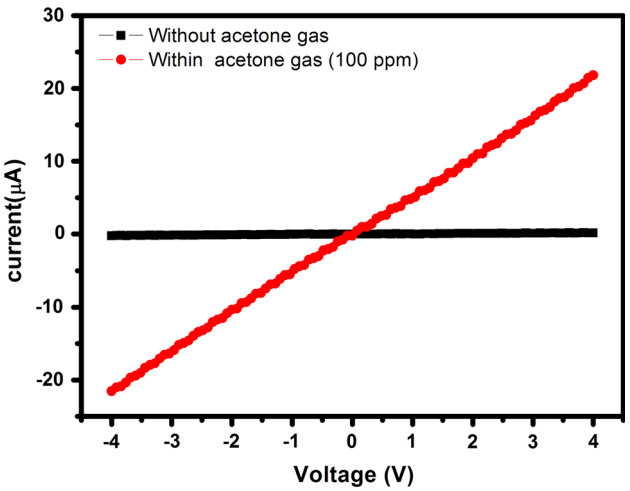

Figure 10 I-V characteristics of 1.0 mol% Fe-SnO_2 sensor before and after acetone (100 ppm) exposure at 200 °C.

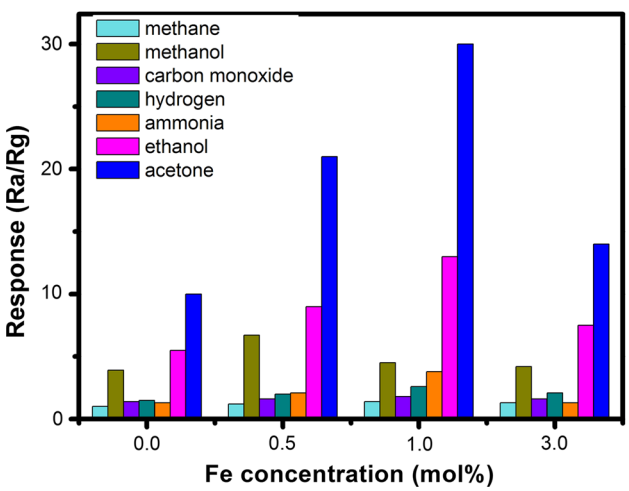

Figure 11 Selectivity of the pure and Fe-doped SnO_2 microstructures sensors to different gases.

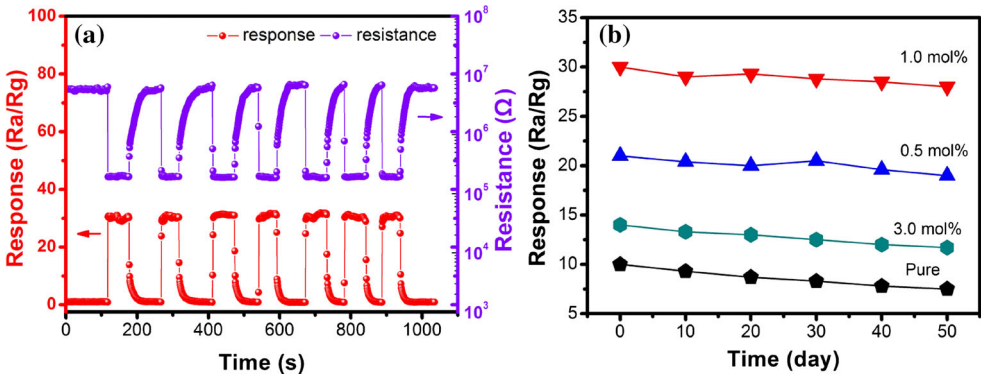

Figure 12 Reversibility of **a** 1.0 mol% Fe-doped SnO_2 sensor toward 100 ppm acetone at 200 °C, **b** long-term stability of as-prepared SnO_2 gas sensors in 50 days, respectively.

Table 1 Acetone sensing performance of typical SnO_2 materials and Fe-doped SnO_2 in this work

Materials	S (C)	T (°C)	LOD	t_{res}/t_{rec}	Ref.
SnO_2 nanoparticles	18 (100 ppm)	240	200 ppb	–/–	[42]
SnO_2 hollow microspheres	30 (160 ppm)	200	5 ppm	5/7 s	[43]
SnO_2 nanopolyhedrons	30 (100 ppm)	370	1 ppm	9.7/5.8 s	[44]
Ce-doped SnO_2 hollow spheres	11.9 (100 ppm)	250	–	18/7 s	[45]
α-Fe_2O_3/SnO_2 composites	16.8 (100 ppm)	250	10 ppm	3/90 s	[46]
ZnO/SnO_2 thin film	1.5 (200 ppm)	250	–	–/–	[47]
Flower-shaped SnO_2 nanostructures	20 (100 ppm)	280	–	–/–	[48]
γ-Fe_2O_3@SnO_2 NPs	8 (100 ppm)	370	10 ppm	6/8 s	[49]
1.0 mol% Fe-doped SnO_2	30 (100 ppm)	200	100 ppb	1/58 s	This work

S response, *C* gas concentration, *T* working temperature, *LOD* limit of detection, $t_{res/rec}$ response/recovery time

demonstrated the highest response to acetone among the other gases.

The reversibility and long-term stability are also very important requirements for the practical application of these sensors. To further investigate the reversibility, cycle sensing experiments were performed on 1.0 mol% Fe-doped SnO_2 acetone sensor as shown in Fig. 12a. After seven cycles between exposure to acetone and fresh air, both the response and resistance can recover to their initial values after removal of acetone, exhibiting an excellent reversibility. Figure 12b shows the long-term stability results measured for 100 ppm acetone every ten days within two months. The measured maximal deviations of the response for 1.0 mol% Fe-doped SnO_2 gas sensor to acetone were <7% over a period of 50 days testing, which illustrated good long-term stability of the developed sensing material for practical applications.

The overall sensing capabilities of the sensor based on the developed 1.0 mol% Fe-doped 3D SnO_2 gas sensing materials are compared with the best previous reports for the SnO_2–based sensors in Table 1. The results indicate that the 1.0 mol% Fe-doped 3D SnO_2 acetone sensor has lowest detection limit (~100 ppb) and operational temperature of 200 °C, high response toward acetone, which clearly demonstrates excellent sensing capabilities for acetone.

Gas sensing mechanism

It is well known that the gas sensing mechanism of an oxide semiconductor is based on the resistance change through the thickness of the depletion layer, which varies according to the amount of oxygen absorbed on the surface [50]. Figure 13 presents schematic illustration of the gas sensing mechanism for pure SnO_2 and Fe-doped SnO_2 3D microstructures to acetone. When the pure SnO_2 microstructures are exposed to air, oxygen molecules can be adsorbed on the SnO_2 surface and ionized to O_2^-, O^-, O^{2-} ions by trapping electrons from the conduction band of SnO_2 (Fig. 13a) [51]. As a result, a charge depletion layer is

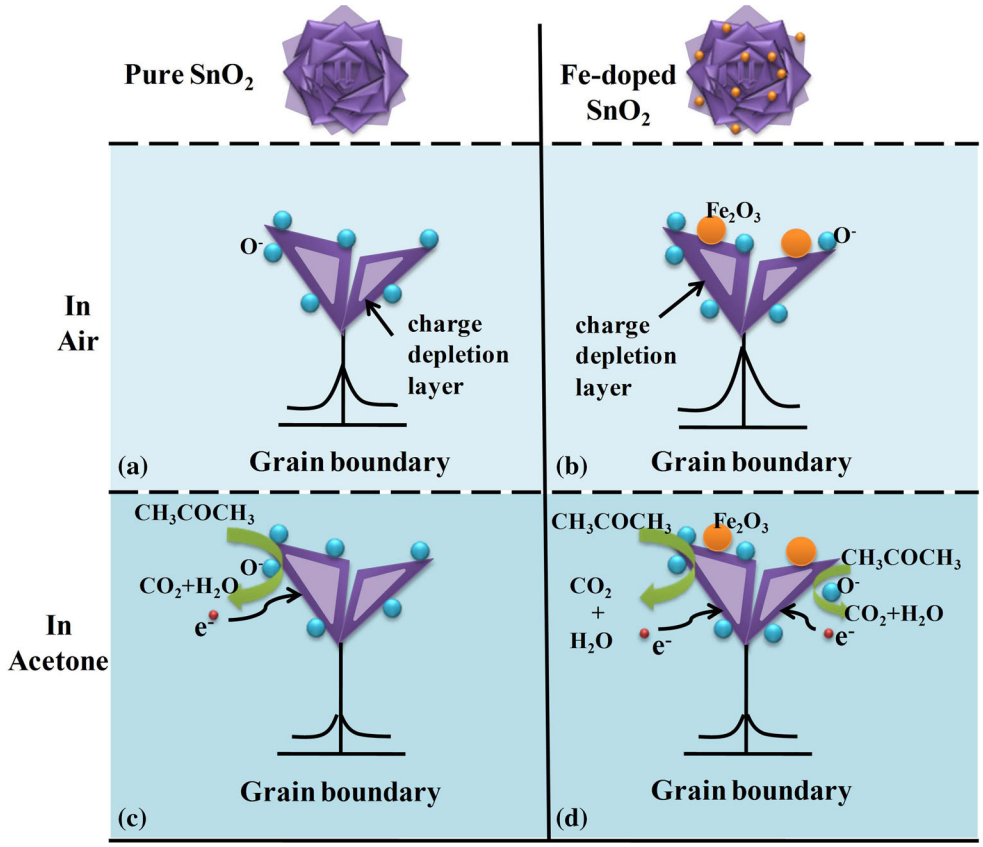

Figure 13 Schematic illustration of the mechanism governing the depletion layer for **a** pure SnO_2 and **b** Fe-doped SnO_2 microstructures in air, **c** pure SnO_2 and **d** Fe-doped SnO_2 microstructures in acetone atmosphere.

generated at the surface of SnO_2, which leads to the increase in its resistance [52]. When material is exposed to the reducing gas (acetone, in this instance), the adsorbed oxygen species react with the acetone and release electrons into the conduction band, which will decline the resistance of the sensor (Fig. 13c). The main reaction on the SnO_2 surface is speculated to be as follows:

$$CH_3COCH_3 + 8O^-_{ads} \rightarrow 3CO_2 + 3H_2O + 8e^-. \quad (1)$$

For the Fe-doped SnO_2 microstructures, the enhanced sensing properties are likely attributed to the introducing of Fe element on the surface of 3D SnO_2 microstructures, which leads to a larger lattice distortion, which ultimately enhances oxygen adsorption and promotes the dissociation process of the molecular oxygen resulting in the greater and faster degree of electron depletion from the SnO_2 microstructures (Fig. 13b) [53]. On the other hand, the heterojunction constituted at the surface between Fe_2O_3 and SnO_2 also enlarges the space charge layer. When the Fe-doped SnO_2-based sensors are exposed to acetone vapor atmosphere, the depleted layer was fading away fast, and the trapped electrons were released back to the conduction band (Fig. 13d). However, when the SnO_2 is over-doped by Fe the response decreases due to the reducing of the available adsorption sites. Therefore, we attribute 1.0 mol% Fe-doped SnO_2 3D microstructure as the optimal doped 3D structure providing maxim sensibility and selectivity toward acetone sensing on the *ppb* level.

Conclusions

Enhancement of the acetone sensing toward the *ppb*-level detection was achieved by modification of the sensing material representing 1.0 mol% Fe-doped 3D SnO_2 hierarchical microstructures. These new 3D microstructures were successfully synthesized and fabricated via one-step hydrothermal method. As-prepared Fe-doped SnO_2 samples consist of 3D flower-like hierarchical microstructures and have no

other impurities, which was subsequently confirmed by the various materials characterization methods. The sensors based on these newly developed 3D microstructures have demonstrated that the Fe-doped of 3D SnO_2 can significantly enhance both response and selectivity of the material toward the acetone measurement at *ppb* level compared with the sensor based on pure SnO_2. It was also experimentally found that the 1.0 mol% Fe-doped SnO_2 microstructures exhibit the highest response, fast response/recovery time, lowest detection limit and good selectivity to acetone at the optimum working temperature of 200 °C. The excellent sensing capabilities are attributed to the particular unique hierarchical morphology and incorporation of Fe_2O_3 to form the heterojunction interface. The obtained results evidently demonstrated that the effective integration of the metal oxide nanoparticles at the right concentration will be very helpful approach for development of new semiconductor sensing materials for various devices.

Acknowledgements

This work was financially supported by the National Natural Science Foundation of China (51205274), Higher school science and technology innovation Project of Shanxi (2016137), Natural Science of Shanxi Province (2016011039), Talent Project of Shanxi Province (201605D211036), Science and Technology Major Project of the Shan Xi Science and Technology Department (20121101004), Key Disciplines Construction in Colleges and Universities of Shanxi ([2012]45).

Electronic supplementary material: The online version of this article (doi:10.1007/s10853-017-1319-8) contains supplementary material, which is available to authorized users.

References

[1] Liu S, Zhang F, Li H, Chen T, Wang Y (2012) Acetone detection properties of single crystalline tungsten oxide plates synthesized by hydrothermal method using cetyltrimethyl ammonium bromide supermolecular template. Sens Actuators, B 162:259–268

[2] Liu X, Hu J, Cheng B, Qin H, Jiang M (2008) Acetone gas sensing properties of $SmFe_{1-x}Mg_xO_3$ perovskite oxides. Sens Actuators, B 134:483–487

[3] Righettoni M, Tricoli A, Pratsinis SE (2010) Si:WO_3 Sensors for highly selective detection of acetone for easy diagnosis of diabetes by breath analysis. Anal Chem 82:3581–3587

[4] Kumar S, Huang J, Abbassi-Ghadi N, ŠPaněL P, Smith D, Hanna GB (2013) Selected ion flow tube mass spectrometry analysis of exhaled breath for volatile organic compound profiling of esophago-gastric cancer. Anal Chem 85:6121–6128

[5] Kamat PC, Roller CB, Namjou K, Jeffers JD, Faramarzalian A, Salas R, Mccann PJ (2007) Measurement of acetaldehyde in exhaled breath using a laser absorption spectrometer. Appl Optics 46:3969–3975

[6] Choi SJ, Lee I, Jang BH, Youn DY, Ryu WH, Park CO, Kim ID (2013) Selective diagnosis of diabetes using Pt-functionalized WO_3 hemitube networks as a sensing layer of acetone in exhaled breath. Anal Chem 85:1792–1796

[7] Tang W, Wang J, Qiao Q, Liu Z, Li X (2015) Mechanism for acetone sensing property of Pd-loaded SnO_2 nanofibers prepared by electrospinning: fermi-level effects. J Mater Sci 50:2605–2615. doi:10.1007/s10853-015-8836-0

[8] Kumar A, Sanger A, Kumar A, Chandra R (2016) Highly sensitive and selective CO gas sensor based on a hydrophobic SnO_2/CuO bilayer. RSC Adv 6:47178–47184

[9] Jain S, Sanger A, Chauhan S, Chandra R (2014) Hydrogen sensing properties of nanostructured Pd/WO_3 thin films: role of hydrophobicity during recovery process. Mater Res Express 1:035046

[10] Sun Y, Chen L, Wang Y, Zhao Z, Li P, Zhang W, Leprince-Wang Y, Hu J (2017) Synthesis of MoO_3/WO_3 composite nanostructures for highly sensitive ethanol and acetone detection. J Mater Sci 52:1561–1572. doi:10.1007/s10853-016-0450-2

[11] Zhu BL, Xie CS, Zeng DW, Wang AH, Song WL, Zhao XZ (2005) New method of synthesizing In_2O_3 nanoparticles for application in volatile organic compounds (VOCs) gas sensors. J Mater Sci 40:5783–5785. doi:10.1007/s10853-005-4562-3

[12] Song P, Wang Q, Yang Z (2012) Acetone sensing characteristics of ZnO hollow spheres prepared by one-pot hydrothermal reaction. Mater Lett 86:168–170

[13] Wang C, Liu J, Yang Q, Sun P, Gao Y, Liu F, Zheng J, Lu G (2015) Ultrasensitive and low detection limit of acetone gas sensor based on W-doped NiO hierarchical nanostructure. Sens Actuators, B 220:59–67

[14] Sanger A, Kumar A, Kumar A, Chandra R (2016) Highly sensitive and selective hydrogen gas sensor using sputtered

grown Pd decorated MnO_2 nanowalls. Sens Actuators, B 234:8–14

[15] Sanger A, Kumar A, Kumar A, Jaiswal J, Chandra R (2016) A fast response/recovery of hydrophobic Pd/V_2O_5 thin films for hydrogen gas sensing. Sens Actuators, B 236:16–26

[16] Liu Y, Jiao Y, Zhang Z, Qu F, Umar A, Wu X (2014) Hierarchical SnO_2 nanostructures made of intermingled ultrathin nanosheets for environmental remediation, smart gas sensor, and supercapacitor applications. Appl Mater Interfaces 6:2174–2184

[17] Lee JH, Katoch A, Choi SW, Kim JH, Kim HW, Kim SS (2015) Extraordinary improvement of gas-sensing performances in SnO_2 nanofibers due to creation of local p–n heterojunctions by loading reduced graphene oxide nanosheets. Appl Mater Interfaces 7:3101–3109

[18] Li L, He S, Liu M, Zhang C, Chen W (2015) Three-dimensional mesoporous graphene aerogel-supported SnO_2 nanocrystals for high-performance NO_2 gas sensing at low temperature. Anal Chem 87:1638–1645

[19] Wu J, Zeng D, Tian S, Xu K, Li D, Xie C (2015) Competitive influence of surface area and mesopore size on gas-sensing properties of SnO_2 hollow fibers. J Mater Sci 50:7725–7734. doi:10.1007/s10853-015-9339-8

[20] Yu YT, Dutta P (2011) Examination of Au/SnO_2 core-shell architecture nanoparticle for low temperature gas sensing applications. Sens Actuators, B 157:444–449

[21] Gao F, Qin G, Li Y, Jiang Q, Luo L, Zhao K, Liu Y, Zhao H (2016) One-pot synthesis of La-doped SnO_2 layered nanoarrays with enhanced gas-sensing performance toward acetone. RSC Adv 6:10298–10310

[22] Zhao Q, Ju D, Deng X, Huang J, Cao B, Xu X (2015) Morphology-modulation of SnO_2 hierarchical architectures by Zn doping for glycol gas sensing and photocatalytic applications. Sci Rep 5:7874

[23] Lou Z, Wang L, Fei T, Zhang T (2012) Enhanced ethanol sensing properties of NiO-doped SnO_2 polyhedra. New J Chem 36:1003–1007

[24] Sun P, Zhou X, Wang C, Wang B, Xu X, Lu G (2014) One-step synthesis and gas sensing properties of hierarchical Cd-doped SnO_2 nanostructures. Sens Actuators, B 190:32–39

[25] Wang Z, Liu L (2009) Synthesis and ethanol sensing properties of Fe-doped SnO_2 nanofibers. Mater Lett 63:917–919

[26] Li X, Zhou X, Guo H, Wang C, Liu J, Sun P, Liu F, Lu G (2014) Design of Au@ ZnO yolk–shell nanospheres with enhanced gas sensing properties. Appl Mater Interfaces 6:18661–18667

[27] Qin G, Gao F, Jiang Q, Li Y, Liu Y, Luo L, Zhao K, Zhao H (2016) Well-aligned Nd-doped SnO_2 nanorods layered array: preparation, characterization and enhanced alcohol-gas sensing performance. Phys Chem Chem Phys 18:5537–5549

[28] Li W, Ma S, Li Y, Li X, Wang C, Yang X, Cheng L, Mao Y, Luo J, Gengzang D (2014) Preparation of Pr-doped SnO_2 hollow nanofibers by electrospinning method and their gas sensing properties. J Alloy Compd 605:80–88

[29] Kim HJ, Choi KI, Pan A, Kim ID, Kim HR, Kim KM, Na CW, Cao G, Lee JH (2011) Template-free solvothermal synthesis of hollow hematite spheres and their applications in gas sensors and Li-ion batteries. J Mater Chem 21:6549–6555

[30] Grosvenor AP, Kobe BA, Biesinger MC, Mcintyre NS (2004) Investigation of multiplet splitting of Fe2p XPS spectra and bonding in iron compounds. Surf Interface Anal 36:1564–1574

[31] Bai S, Hu J, Li D, Luo R, Chena A, Liu CC (2011) Quantum-sized ZnO nanoparticles: synthesis, characterization and sensing properties for NO_2. J Mater Chem 21:12288–12294

[32] Wei S, Zhou M, Du W (2011) Improved acetone sensing properties of ZnO hollow nanofibers by single capillary electrospinning. Sens Actuators, B 160:753–759

[33] Sahay PP, Nath RK (2008) Al-doped ZnO thin films as methanol sensors. Sens Actuators, B 134:654–659

[34] Li X, Zhou X, Guo H, Wang C, Liu J, Sun P, Liu F, Lu G (2014) Design of Au@ZnO yolk-shell nanospheres with enhanced gas sensing properties. Appl Mater Interfaces 6:18661–18667

[35] Chen D, Xu J, Xie Z, Shen G (2011) Nanowires assembled SnO_2 nanopolyhedrons with enhanced gas sensing properties. Appl Mater Interfaces 3:2112–2117

[36] Liu C, Zhao L, Wang B, Sun P, Wang Q, Gao Y, Liang X, Zhang T, Lu G (2017) Acetone gas sensor based on NiO/ZnO hollow spheres: fast response and recovery, and low (ppb) detection limit. J Colloid Interface Sci 495:207–215

[37] Choi KI, Kim HJ, Kang YC, Lee JH (2014) Ultraselective and ultrasensitive detection of H_2S in highly humid atmosphere using CuO-loaded SnO_2 hollow spheres for real-time diagnosis of halitosis. Sens Actuators, B 194:371–376

[38] Zhang L, Zhao J, Lu H, Li L, Zheng J, Li H, Zhu Z (2012) Facile synthesis and ultrahigh ethanol response of hierarchically porous ZnO nanosheets. Sens Actuators, B 161:209–215

[39] Wang H, Qu Y, Chen H, Lin Z, Dai K (2014) Highly selective n-butanol gas sensor based on mesoporous SnO_2 prepared with hydrothermal treatment. Sens Actuators, B 201:153–159

[40] Zhou X, Liu J, Wang C, Sun P, Hu X, Li X, Shimanoe K, Yamazoe N, Lu G (2015) Highly sensitive acetone gas sensor based on porous $ZnFe_2O_4$ nanospheres. Sens Actuators, B 206:577–583

[41] Zhang Z, Zhu L, Wen Z, Ye Z (2017) Controllable synthesis of Co_3O_4 crossed nanosheet arrays toward an acetone gas sensor. Sens Actuators, B 238:1052–1059

[42] Li L, Lin H, Qu F (2013) Synthesis of mesoporous SnO_2 nanomaterials with selective gas-sensing properties. J Sol-Gel Sci Techn 67:545–555

[43] Li J, Tang P, Zhang J, Feng Y, Luo R, Chen A, Li D (2016) Facile synthesis and acetone sensing performance of hierarchical SnO_2 hollow microspheres with controllable size and shell thickness. Ind Eng Chem Res 55:3588–3595

[44] Chen D, Xu J, Xie Z, Shen G (2011) Nanowires assembled SnO_2 nanopolyhedrons with enhanced gas sensing properties. Appl Mater Interfaces 3:2112–2117

[45] Song P, Wang Q, Yang Z (2012) Preparation, characterization and acetone sensing properties of Ce-doped SnO_2 hollow spheres. Sens Actuators, B 173:839–846

[46] Sun P, Cai Y, Du S, Xu X, You L, Ma J, Liu F, Liang X, Sun Y, Lu G (2013) Hierarchical α-Fe_2O_3/SnO_2 semiconductor composites: hydrothermal synthesis and gas sensing properties. Sens Actuators, B 182:336–343

[47] Kim KW, Cho PS, Kim SJ, Lee JH, Kang CY, Kim JS, Yoon SJ (2007) The selective detection of C_2H_5OH using SnO_2–ZnO thin film gas sensors prepared by combinatorial solution deposition. Sens Actuators, B 123:318–324

[48] Huang J, Yu K, Gu C, Zhai M, Wu Y, Yang M, Liu J (2010) Preparation of porous flower-shaped SnO_2 nanostructures and their gas-sensing property. Sens Actuators, B 147:467–474

[49] Zhang S, Ren F, Wu W, Zhou J, Xiao X, Sun L, Liu Y, Jiang C (2013) Controllable synthesis of recyclable core–shell γ-Fe_2O_3@SnO_2 hollow nanoparticles with enhanced photocatalytic and gas sensing properties. Phys Chem Chem Phys Pccp 15:8228–8236

[50] Wen W, Wu JM, Wang YD (2012) Large-size porous ZnO flakes with superior gas-sensing performance. Appl Phys Lett 100:262111–262114

[51] Xu J, Chen Y, Chen D, Shen J (2006) Hydrothermal synthesis and gas sensing characters of ZnO nanorods. Sens Actuators, B 113:526–531

[52] Kaneti YV, Yue J, Jiang X, Yu A (2013) Controllable synthesis of ZnO nanoflakes with exposed (1010) for enhanced gas sensing performance. J Phys Chem C 117:13153–13162

[53] Zhang T, Chen M, Gu F, Han D, Wang Z, Guo G (2012) Alcohol sensing properties of Er-doped In_2O_3 hollow spheres. Integr Ferroelectr 138:117–122